α-particle optical potential tests below the Coulomb barrier

M. Avrigeanu and V. Avrigeanu*

"Horia Hulubei" National Institute for Physics and Nuclear Engineering, P. O. Box MG-6, Bucharest-Magurele, Romania

(Received 4 November 2008; revised manuscript received 30 December 2008; published 5 February 2009)

The results of two recent papers concerning (α,γ) and (α,n) reaction cross sections close to the reaction thresholds are discussed with regard to predictions of a recent α-particle regional optical potential. It is found that the new measured cross sections are rather well described especially for the dominant reaction channels. Particular features of the α-particle optical potential at energies below the Coulomb barrier explain the failure of a former regional potential obtained by analysis of α-particle elastic scattering alone at higher energies. Additional limitations of statistical model calculations for minor reaction channels are also discussed.

DOI: 10.1103/PhysRevC.79.027601 PACS number(s): 24.10.Ht, 24.60.Dr, 25.55.−e, 27.60.+j

I. Motivation. Two recent studies of (α,n) reactions on ^{92,94}Mo isotopes and α capture on ^{112}Sn [1] and ^{117}Sn [2] were also motivated by the still poor knowledge of the α-particle optical model potential (OMP) below the Coulomb barrier. Thus Rapp *et al.* [1] performed useful comparisons of the new measured data and statistical model calculations with different optical potentials, including a former regional parameter set [3] established by analysis of the α-particle elastic scattering alone. Their results emphasized either a data overestimation by a factor of 2 or an underestimation by a similar factor. On the other hand, additional limitations of the OMP parameters, the more recent being again that of Ref. [3], were found below the Coulomb barrier and considered typical for the available global OM parametrizations [2]. We provide an additional account of the new measured cross sections [1,2] by means of a recent optical potential [4] to check whether it also describes these data.

In the first place, we think it is important to emphasize the particular precondition and aims of our former optical potential [3] that was used in Refs. [1,2]. First, we had focused on two main questions that are still open, namely, the OMP parameter sets obtained from α-particle elastic scattering at high energies ($E_\alpha > 80$ MeV), which describe neither the lower-energy (<40 MeV) elastic scattering nor the complete fusion data, and the statistical α-particle emission that is underestimated by the OMPs that account for elastic scattering on the ground-state nuclei ([5] and references therein). As stated from the beginning in Ref. [3], we started with the analysis of the α-particle elastic scattering alone, for nuclei in the mass region $A \sim 100$ and energies from ∼14 to 32 MeV, while an eventual failure to describe reaction data remained to be understood later. At the same time we did not take into account either the available experimental α-induced or the (n,α) reaction cross sections, to avoid additional difficulties because of the remaining parameters needed in statistical model calculations [6]. Thus, the potential of Ref. [3] has been less suitable for the analysis of the new data measured at incident energies $E_\alpha \approx 8$–15 MeV [1,2], i.e., outside the energy range involved for its setting up.

A further step concerning the α-induced reactions below the Coulomb barrier B has recently been carried out [4] while the eventual difference of α-particle potentials in the entrance/exit channels [5] has yet to be understood. Basically, the regional optical potential (ROP) based entirely on α-particle elastic scattering [3] was extended to $A \sim 50$–120 nuclei and energies from ∼13 to 50 MeV. Then, an ultimate assessment of available (α,γ), (α,n), and (α,p) reaction cross sections that concerned target nuclei from ^{45}Sc to ^{118}Sn and incident energies below 12 MeV was carried out. Because the Coulomb barrier rules out elastic scattering measurements at lower energies, the analysis of reaction cross sections within this energy range is indeed the only way to validate the related accuracy of an α-particle optical potential. Thus, the diffuseness a_R of the real part of the optical potential as well as the surface imaginary potential depth W_D, established by the former analysis above B, has been found to be responsible for the actual difficulties in the description of the reaction data below B. Consequently, their energy dependence has been modified for $E_{\mathrm{c.m.}}/B < 0.9$ (Table 3 of Ref. [4]) to obtain an optical potential that describes equally well the low energy α-particle-induced reaction and elastic scattering data.

II. The (α,x) reactions on ^{92,94}Mo and ^{112}Sn. The new data of Rapp *et al.* [1] are compared in Figs. 1(a)–1(c) with the results of statistical model calculations using a consistent input parameter set [4,5] except the α-particle optical potential. In this case we have used both the ROP parameter values provided by the only elastic scattering analysis above B, and the above-mentioned a_R and W_D energy dependencies proved to be correct at the energies below B, to point out the improvement due to the previous reaction data analysis [4]. The α-particle total reaction cross sections in the former instance are also compared with the results of the previous ROP form [3] involved in Refs. [1,2], to be aware of their proximity. In addition, all reaction-channel cross sections calculated using the complete ROP [4] are compared in Figs. 1(d)–1(f).

The overall good agreement between the measured and calculated cross sections for the major α-induced reaction channels, except an (α,n) data overestimation around the incident energy of ∼10.5 MeV (Fig. 1), provides a trustworthy confirmation of the related α-particle ROP [4]. It results especially from the suitable description of the (α,n) reaction cross section within the so critical energy range just above the threshold. This point as well as the reproduction of the energy dependence of new data for the reaction ^{94}Mo$(\alpha,n)^{97}$Ru was proven in Fig. 2 of Ref. [1] to be real challenges for statistical model calculations. The same figure showed larger differences between the experimental and calculated cross sections for the reaction ^{112}Sn$(\alpha,\gamma)^{116}$Te, which is confirmed in Fig. 1(c)

*vavrig@ifin.nipne.ro

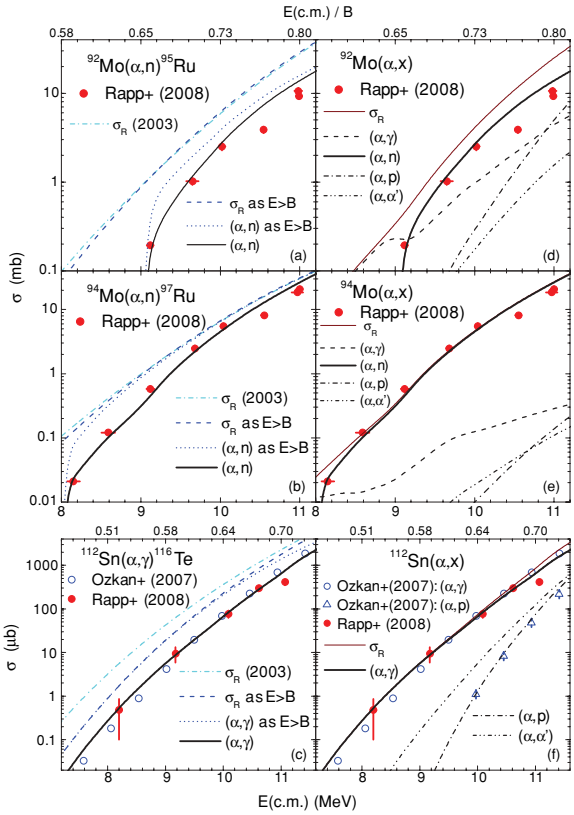

FIG. 1. (Color online) Comparison of (a)–(c) calculated total α-reaction cross sections using a former ROP [3] (dash-dotted curves) and parameters in Ref. [4] obtained above the Coulomb barrier height B, in MeV ($E > B$), by elastic scattering analysis alone (dashed curve). Comparison of the measured cross sections for (α,n) reaction on ^{92,94}Mo nuclei [1], and (α,γ) and (α,p) reactions on ^{112}Sn [1,7], and calculated values using (a)–(c) ROP parameters at $E > B$ (dotted curves) and complete ROP [4] (solid), and (d)–(f) the complete ROP.

by using also the ROP parameters established only above B. This increased divergence is related to the incident energies involved with respect to B lower than those for Mo isotopes, while a larger negative Q value by 4 MeV for the (α,n) reaction pushes its threshold beyond these energies so that the (α,γ) reaction becomes the dominating channel. Therefore it is important that these particular data are better described by the final ROP of Ref. [4], together with the (α,γ) and (α,p) reaction data of Ref. [7]. The latter was used in the determination of the ROP [4].

With regard to the overestimation especially for the ^{92}M$(\alpha,n)^{95}$Ru reaction cross section around the incident energy of ~10.5 MeV, one should consider the following points. It is true that the sensitivity of the calculated (α,n) cross sections to the neutron widths is usually higher only close to the reaction threshold but is almost exclusively given by the α width at higher energy [1]. However, the particular low-lying level structure of the residual nucleus ^{95}Ru, with the neutron number $N = 51$, triggered 77% of the side-feeding cross section at this incident energy to its ground state (g.s.), based on the most recent knowledge [8] of the ^{95}Ru levels (Table I) observed in (α,xn) reactions. Also the larger negative Q value makes this reaction channel dominate the others by a factor of only ~3 around 10.5 MeV, in comparison with nearly two orders of magnitude for ^{94}Mo [Figs. 1(d) and 1(e)]. Thus, any less accurate knowledge of level schemes and model parameters other than α-particle OMP, or the eventual missing account of a nonstatistical nuclear process, may lead to this data overestimation.

III. Analysis of (α,x) reactions on ^{117,118}Sn. A quite different case is that of the (α,γ) and (α,p) reactions on ^{117}Sn [2] within an incident energy range that is closer to, although still below, B. The related (α,n) reaction Q value being almost half of that for the ^{112}Sn target nucleus, this reaction channel is by far the strongest at these energies, e.g., Figs. 2(a) and 2(b). Under these circumstances the differences in Fig. 2(a) between the reaction cross sections calculated by using the α-particle optical potentials based on the elastic scattering analysis above B, and those taking into account the reaction data as well [4], are already rather small. On the other hand, the disagreement between the measured data and the calculated values goes up by over an order of magnitude for both minor reaction channels. It is compared in Fig. 2(c) with the case of the ^{118}Sn$(\alpha,\gamma)^{122}$Te reaction [9], already considered in Ref. [4]. The similar minor character of the radiative capture channel, despite an (α,n) reaction negative Q value ~2 MeV higher, is shown in Fig. 2(d). However, the above-mentioned disagreement mainly concerns in this case the slope of the (α,γ) excitation function. Therefore, we examined again statistical model parameters formerly adopted [4].

A. Model parameters. Actually, from the very beginning we have striven for a better knowledge of the neutron OMP and γ-ray strength functions focusing on the analysis of neutron total cross sections for all Sn and Te stable isotopes as well as on the neutron capture on the same target nuclei [10]. Consequently, we found that the global and local neutron OMPs of Koning and Delaroche [11] describe well the

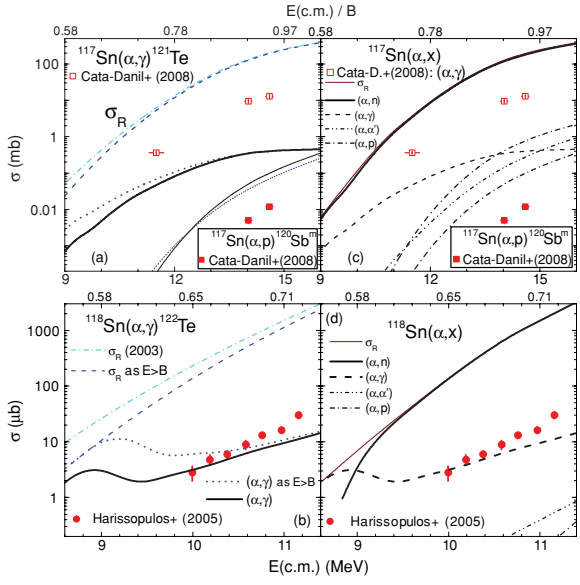

FIG. 2. (Color online) The same as in Fig. 1 but for the (α,γ) reaction on (a,c) ^{117}Sn [2] and (b,d) ^{118}Sn [9] nuclei, as well as (a) ^{117}Sn$(\alpha,p)^{120}$Sb^m reaction [2] and calculations using ROP parameters established at $E > B$ (thin dotted curve) and complete ROP [4] (thin solid curve), and (c) both the total and isomeric state populations by the (α,p) reaction (upper and lower dash-dotted curves, respectively).

TABLE I. Low-lying level number N_d up to excitation energy E_d [8] used in cross-section calculations, and the levels and s-wave neutron-resonance spacings $D_0^{\exp}$ in the energy range ΔE above the separation energy S, for the target-nucleus g.s. spin I_0, fitted to obtain the BSFG level density parameter a and g.s. shift Δ (for a spin cutoff factor calculated with a variable moment of inertia between half and 75% of the rigid-body value, from g.s. to S, and reduced radius $r_0 = 1.25$ fm).

Nucleus	N_d	E_d (MeV)	Fitted level and resonance data					a (MeV^{-1})	Δ (MeV)
			N_d	E_d (MeV)	$S + \frac{\Delta E}{2}$ (MeV)	I_0	$D_0^{\exp}$ (MeV)		
^{95}Ru	9	2.493	17	2.54				11.00	0.62
^{97}Ru	17	1.620	17	1.62				11.70	−0.16
^{112}Sn	21	2.989	21	2.99				13.85	1.34
^{117}Sn	21	1.710	21	1.71	11.059	0	0.38(13)	13.80	0.12
^{118}Sn	38	3.057	38	3.06	9.326	1/2	0.055(5)	13.55	1.10
^{115}Sb	11	1.755	11	1.76				14.20	0.45
^{120}Sb	21	0.448	21	0.45				13.75	−1.35
^{121}Sb	23	1.659	23	1.66				14.00	0.10
^{115}Te	3	0.280	3	0.28				14.40	−0.45
^{116}Te	11	2.119	11	2.12				14.00	0.80
^{120}Te	20	2.461	20	2.46				14.00	0.87
^{121}Te	20	0.830	29	1.02				14.30	−0.72
^{122}Te	25	2.594	25	2.59				14.20	0.94

more recent data of the total neutron cross sections for Sn isotopes, but in the limit of ∼15% underestimation for Te isotopes. To avoid this uncertainty, the local OMP parameter set for the isotope ^{128}Te was adopted together with the use of Fermi-energy global values [11] for each Te isotope. A suitable description of the corresponding neutron resonance data [12] was also checked. Next, these neutron OMPs were involved within the neutron capture analysis for all stable isotopes of Sn and Te, for the neutron energies up to 3 MeV, at the same time with recently obtained [13] nuclear level density parameters. Actually the systematical analysis of this neutron-capture data basis was carried out to adopt a suitable normalization of accurate γ-ray strength functions [10] by means of independent experimental information. Concerning the nuclear level density, the back-shifted Fermi gas (BSFG) formula was used for the excitation energies below the neutron-separation energy, with the parameters a and Δ obtained by a fit of the recent experimental low-lying discrete levels [8] and s-wave nucleon resonance spacings D_0 [12]. The smooth-curve method was adopted [14] for nuclei without resonance data, leading to a values of the even-even, odd-odd, and odd-mass nuclei that were next kept fixed during the fit of low-lying discrete levels. The eventually updated parameters are given in Table I together with the fitted data.

B. Proton-emission channel OMP. Having obtained an overestimation of the measured ^{117}Sn$(\alpha,p)^{120}$Sb^m reaction cross sections, we decided to focus on the proton OMP that describe the proton emission from the compound nucleus ^{121}Te. The only independent data available in this respect concern, as usual, the incident channel and alternatively the compound nucleus ^{122}Te, i.e., the ^{121}Sb$(p,n)^{121}$Te^{g,m} reaction cross sections [15]. At sub-Coulomb energies and also above the neutron threshold the neutron emission is the dominant one (Fig. 3). Therefore its model calculation sensitivity to the proton OMP is largest at the energies of these data. Moreover, in Fig. 3(a) it is shown that use of the global proton OMP [11] corresponds to an increase of the (p,n) reaction cross sections with the incident energy a bit larger than that for the measured data. We have found that the adoption of the global parameter set of Johnson, Galonsky, and Kernell [16], with a depth $W_D = 8$ MeV of the OMP surface imaginary part in agreement with its anomalous trend shown in Fig. 17 of Ref. [16], has been an easy way to overcome this minor drawback. However, this change of the proton OMP corresponds to a decrease below 2% of the analyzed (α,p) reaction cross section. On the other hand, this analysis validates, by means of the related isomeric cross-section ratio also shown in Fig. 3(a), the γ-decay scheme of the ^{121}Te nucleus and level density angular-momentum distribution given by the assumed moment of inertia. This point is particularly useful for the model parameters check because the g.s. ($1/2^+$, 19.16 d) and the isomeric state ($11/2^-$, 154 d) of the same nucleus ^{121}Te are also populated through the (α,γ) reaction.

C. The ^{117}Sn$(\alpha,\gamma)^{121}$Te *reaction.* We have also compared the α-induced reaction cross sections, calculated in the present work for the target nucleus ^{117}Sn by using a local parameter set, and results of the standard model calculations performed with the well-known computer codes NON-SMOKER [17] and TALYS-1.0 [18]. The global model parameters described within

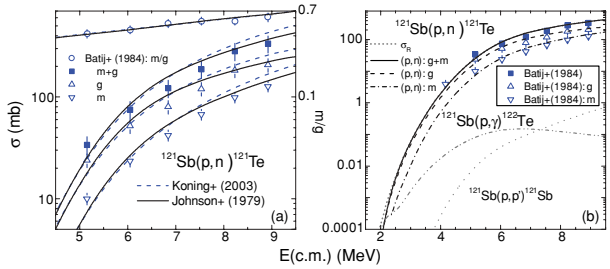

FIG. 3. (Color online) Comparison of measured (p,n) reaction cross sections and isomeric cross-section ratio for ^{121}Sb target nucleus [15] and calculated values using: (a) proton global OMPs of Ref. [11] (dashed curves) and [16] (solid curves), and (b) the latter OMP for the proton reaction cross section (short-dotted curve); the (p,n) total (solid curve), g.s. (dashed curve), and isomeric state (dash-dotted curve) population cross sections; and the (p,γ) reaction (dash-dot-dotted curve) and (p,p') reaction (dotted curve) cross sections.

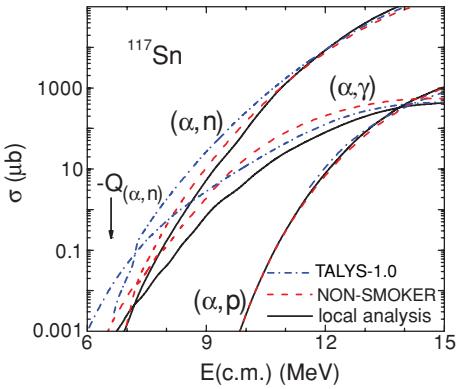

FIG. 4. (Color online) Comparison of (α,γ), (α,n), and (α,p) reaction cross sections calculated by using NON-SMOKER [17] (dashed curves) and TALYS-1.0 [18] (dash-dotted curves) predictions and a local parameter analysis [4] (solid curves).

the same references were used in the latter case, so that their results are firstly predictions of the reaction cross sections. However, larger differences between these results have been found at lower energies, around and within 4–5 MeV above the (α,n) reaction threshold (Fig. 4). Nevertheless, even under such conditions, a common feature is the energy within less than 1 MeV above this threshold (related to $Q = -6.64$ MeV), where the compound nucleus may deexcite rather equally through γ-ray and neutron emissions. Conversely, the normalization used in Ref. [2] to provide a description of the ^{117}Sn$(\alpha,\gamma)^{121}$Te measured data with the calculation led to similar (α,γ) and (α,n) reaction cross sections at an incident energy of ~10 MeV. It follows that the normalization method is leading to unphysical results. We would rather conclude that this disagreement may be due to an overlooked process such as the nonstatistical γ emission. The direct radiative capture in α-induced reactions was formerly pointed out at $E_\alpha \approx$ 10–27 MeV [19,20]. Moreover, favorable conditions for nonnegligible direct capture [21] are met for α-particle capture on ^{117}Sn because the compound nucleus is formed at low excitation energy with a low level density, typical for nuclei near closed shells. In particular, it has been shown that nonequilibrium α-particle captures involve α particles with energies of 10–12 MeV [22], which is consistent with the energy range discussed in this work, especially for the ^{117}Sn nucleus. The related effects should be also less important for ^{118}Sn because of an even smaller weight of the radiative capture (Fig. 2).

D. The ^{117}Sn$(\alpha,p)^{120}$Sb *reaction.* The inclusion of an overlooked direct interaction would lead to a decrease of the α-particle compound reaction cross section. However, because the neutron emission is prevailing by orders of magnitude as shown in Fig. 3(b), this will not be followed by a real change of the (α,p) reaction cross sections. The large overestimation of the measured data could be reduced by, e.g., the decrease of the negative backshift Δ of the residual nucleus ^{120}Sb (Table I) by 200 keV, a similar decrease of Δ for the ^{120}Te nucleus, and an increase of the ^{120}Te level density parameter a by 12.5%. The (α,p) reaction cross sections lower by ~27, 22, and 69%, respectively, would be thus closer to the measured data. However, these parameter changes would be at large variance with the above-mentioned consistency of adopted model parameter set, and therefore they should need additional confirmation.

IV. Conclusions. Limitations of statistical model calculations for minor reaction channels are shown to be most likely due to an overlooked process or critical values of statistical model parameters around closed shells. Nevertheless the α-particle optical potential is not at the origin of these problems, while the new data for ^{92,94}Mo and ^{112}Sn nuclei support the recent potential [4].

This work was supported by CNCSIS Contract No. 149/2007.

[1] W. Rapp, I. Dillmann, F. Käppeler, U. Giesen, H. Klein, T. Rauscher, D. Hentschel, and S. Hilpp, Phys. Rev. C **78**, 025804 (2008).
[2] I. Căta-Danil *et al.*, Phys. Rev. C **78**, 035803 (2008).
[3] M. Avrigeanu, W. von Oertzen, A. J. M. Plompen, and V. Avrigeanu, Nucl. Phys. **A723**, 104 (2003).
[4] M. Avrigeanu, A. C. Obreja, F. L. Roman, V. Avrigeanu, and W. von Oertzen, At. Data Nucl. Data Tables (accepted for publication); arXiv:0808.0566.
[5] M. Avrigeanu, W. von Oertzen, and V. Avrigeanu, Nucl. Phys. **A764**, 246 (2006).
[6] P. Demetriou, C. Grama, and S. Goriely, Nucl. Phys. **A707**, 253 (2002).
[7] N. Özkan *et al.*, Phys. Rev. C **75**, 025801 (2007).
[8] Evaluated Nuclear Structure Data File (ENSDF), www.nndc.bnl.gov/ensdf/.
[9] S. Harissopulos *et al.*, J. Phys. G: Nucl. Part. Phys. **31**, S1417 (2005).
[10] V. Avrigeanu *et al.*, EC Report EUR 23235EN, 2008, p. 143; http://www.irmm.jrc.be/html/publications/technical_reports/publications/EUR23235EN_NEMEA4.pdf.
[11] A. J. Koning and J. P. Delaroche, Nucl. Phys. **A713**, 231 (2003).
[12] IAEA-CRP Reference Input Parameter Library (RIPL-2), http://www-nds.iaea.or.at/RIPL-2/.
[13] V. Avrigeanu, T. Glodariu, A. J. M. Plompen, and H. Weigmann, J. Nucl. Sci. Technol. **S2**, 746 (2002); http://tandem.nipne.ro/~vavrig/publications/2002/Tables/caption.html.
[14] C. H. Johnson, Phys. Rev. C **16**, 2238 (1977).
[15] V. G. Batij *et al.*, EXFOR Nuclear Reaction Data File A0203, dated 1983-12-14; www-nds.iaea.or.at/exfor/.
[16] C. H. Johnson, A. Galonsky, and R. L. Kernell, Phys. Rev. C **20**, 2052 (1979).
[17] T. Rauscher and F.-K. Thielemann, At. Data Nucl. Data Tables **79**, 47 (2001).
[18] A. J. Koning, S. Hilaire, and M. C. Duijvestijn, in *Proceedings International Conference on Nuclear Data for Science and Technology, Nice, 2007*, edited by O. Bersillon *et al.* (EDP Sciences, Paris, 2008), p. 211, http://nd2007.edpsciences.org.
[19] K. Raghunathan, L. L. Rutledge, R. E. Segel, and L. Meyer-Schützmeister, Phys. Rev. C **22**, 2409 (1980).
[20] J. A. Behr, K. A. Snover, C. A. Gossett, G. Feldman, J. H. Gundlach, and M. Kicińska-Habior, Phys. Rev. C **53**, 1759 (1996).
[21] T. Rauscher, J. Phys. G: Nucl. Part. Phys. **35**, 014026 (2007).
[22] T. Rauscher, Phys. Rev. C **78**, 032801(R) (2008).